SLOW MIGRATION OF BRINE INCLUSIONS IN FIRST-YEAR SEA ICE*

NOA KRAITZMAN†, KEITH PROMISLOW‡, AND BRIAN WETTON§

Abstract. We derive a thermodynamically consistent model for liquid-solid phase change in sea ice by incorporating a phase sensitive scalar to a classical framework of liquid-solid phase change. The entropy of the scalar is taken relative to the liquid molar fraction which induces a chemotactic behavior. This provides a transparent mechanism for the rejection of the scalar under formation of the solid phase. We identify slow varying coordinates, including the scalar density relative to liquid molarity weighted by latent heat, and use multiscale analysis to derive a quasi-equilibrium Stefan-type problem via a sharp interface scaling. The singular limit is underdetermined, and the leading order system is closed by imposing local conservation of the scalar under interface perturbation. The quasi-steady system determines interface motion as balance of curvature, temperature gradient, and scalar density. We resolve this numerically for axisymmetric surfaces and show that the thermal gradients typical of arctic sea ice can have a decisive impact on the mode of pinch-off of cylindrical brine inclusions and on the size distribution of the resultant spherical shapes. The density and distribution of these inclusion sizes is a key component of sea ice albedo which factors into global climate models.

1. Introduction. Sea ice plays a significant role in ocean circulation and more broadly in the Earth's weather and climate system. At a global scale sea ice is a thin interfacial layer between the atmosphere and the ocean that serves to reduce evaporation, reflect sunlight, and insulate the ocean from heat loss. At a microscale sea ice is a highly complex, multicomponent system composed of crystalline ice, liquid brine inclusions, air bubbles, and salt precipitate. This work focuses on brine inclusions. They play a leading role in sea ice microstructure, particularly determining its electromagnetic and mechanical properties, creating habitat for a variety of CO_2-binding microalgae [14], and driving the oceanic transport of carbon, nutrients, and salt [9]. Indeed, the fluid flow that arises from the onset of percolation of brine channels leads to both significant downwelling of brine-laden water and an important increase in the effective thermal conductivity of sea ice. Sea ice's albedo, the percentage of solar radiation reflected, is greatly impacted by the surface area density of brine inclusions [25]. Both albedo and effective thermal conductivity of sea ice are key parameters in global circulation models.

Sea ice samples are widely characterized by their age—first year or multiyear—and the temperature and depth below the ice-air surface at which they were harvested.

†Mathematical Sciences Institute, Australian National University, Canberra ACT 2601, Australia (noa.kraitzman@anu.edu.au).

‡Department of Mathematics, Michigan State University, East Lansing, MI 48824 United States (kpromisl@math.msu.edu).

§Department of Mathematics, University of British Columbia, Vancouver, BC V6T 1Z4, Canada (wetton@math.ubc.ca).
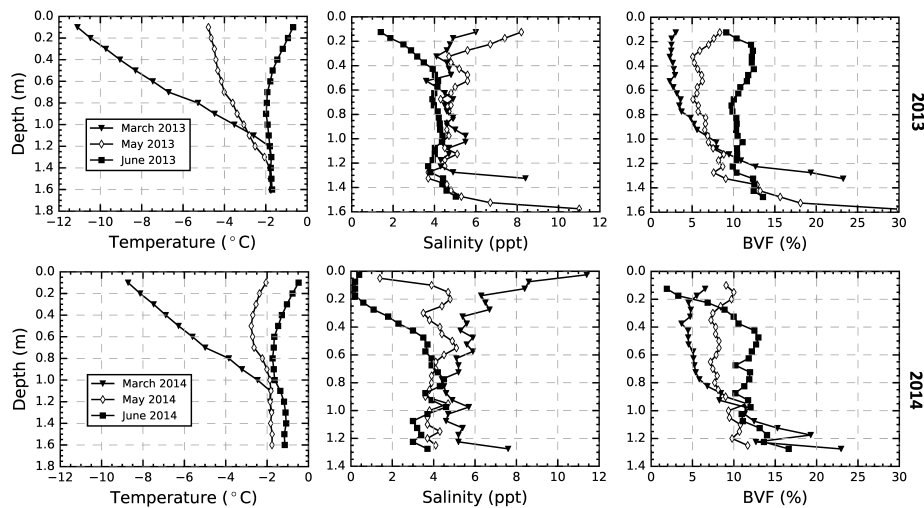
FIG. 1. *Measurements of temperature, bulk salinity (in parts per thousand), and brine volume fraction as a function of depth in arctic sea ice at three different seasonal periods over two years (From [23]; reprinted with permission from creative commons).*

The top row of images in Figure 1, from [23], show the temperature distribution in sea ice at three different seasonal periods over two years. In a given season, the temperature is largely a function of depth while the temperature gradient is spatially uniform in the winter, except at the bottom (ice-water interface) of the ice sheet. The bulk salinity, shown in the second row, is the salt weight fraction, in parts per thousand (ppt), of the total weight including the ice phase. The bulk salinity generically decays at the air-ice surface after the ice has been warmed but remains relatively constant in the middle of the sheet. The brine volume fraction, calculated here from x-ray microtomography, increases with seasonal temperature shifts but less so at the air-ice surface. While the data are noisy, "pore salinity," the salt content of the brine within the inclusions, satisfies an underlying relation. The pore salinity can be postprocessed from this data by approximating the salt density in the ice phase as zero to leading order [30], and dividing the bulk salt density by the brine volume fraction. The results, reported in Figure 2, present temperature and pore salinity parametrically by depth for the three data sets with the largest temperature gradient. Despite incorporating data from a wide range of brine structures throughout the ice-sheet, the plots are in strong agreement with the cryoscopic rule of thumb which relates a 0.54 °C decrease in freezing temperature of water per 1% increase in salt weight fraction (dotted line). The combination of salt ejection from ice and the raising of the freezing point of liquid water with salinity generates a chemotactic process forming spatially extended liquid brine inclusions.

The structure of brine inclusions is well known to be temperature-dependent. As sea ice temperature rises, brine inclusions expand and may interconnect. As ice temperatures fall, inclusions shrink and pores may pinch off into isolated inclusions of various shapes whose diameters range from 0.1 to 10 millimeters [19, 26]. While there is an increasing interest in brine inclusions and sea ice structure [7, 1, 16], there are few mathematical models that incorporate the chemotactic role of salt ejection from ice and the cryoscopic relation between salt density and freezing point. There is a rich mathematical literature on phase change that incorporates latent heat, including
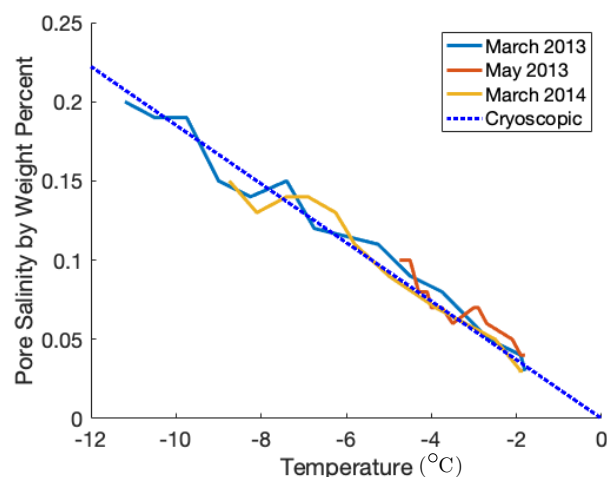
FIG. 2. *Pore salinity computed as the ratio of bulk salinity and brine volume fraction for the three data sets (from Figure 1) with the largest temperature gradient. The pore salinity is plotted verses temperature (parametrically in depth) and compared to the linear approximation of the cryoscopic relation (dotted line).*

[2] which presents scaling connections to many standard models. The work of [6] incorporates salt into a very general thermodynamic model with a strong emphasis on the elastic energy of the mixture; however this approach is technical and does not provide a transparent physical mechanism for salt ejection from ice. The work [21] incorporates models for the nanoscale structure of water networks and the role of salt in destabilizing them but is not presented in the context of a thermodynamically consistent model.

We present a thermodynamically consistent phase-field model for the formation and evolution of brine inclusions within ice that rests upon a simple mechanism for salt exclusion. The model incorporates an entropy production mechanism that conserves internal energy. This follows the GENERIC framework for thermodynamic consistency developed by Grmela and Öttinger [10, 11] and placed into a framework more accessible to a broader mathematical audience by Mielke [20]. More specifically we incorporate salt into the entropy based models of phase change presented by Penrose and Fife [24]. Salt exclusion arises naturally by taking the entropy of the salt relative to the density of liquid-phase water molecules. The liquid water molecules solvate the salt ions, and their removal by the freezing process unfavorably decreases the entropy of the ions. The resulting ejection of salt from the regions of freezing engenders a chemotactic flow for the salt density that leads to the development of spatially extended regions of high salt concentration—the brine inclusions.

We consider a scaling of the model which recovers a sharp-interface limit for the ice-liquid interface, while maintaining a finite latent heat of phase change. The singular nature of the relative entropy of the salt precludes smooth transitions in salinity across the ice-water front. We overcome this by reformulating the system in terms of phase, temperature, and salt density relative to liquid phase and show that this relative density is smooth. We present a multiscale analysis that derives a Stefan-type problem (explicit moving boundary) for the evolution of the brine-ice front coupled to temperature, salinity, and interfacial curvature. However, because of the salt ejection the Stefan-type problem is formally underdetermined at leading order. We use conservation of salt under front perturbations to derive a boundary condition that closes
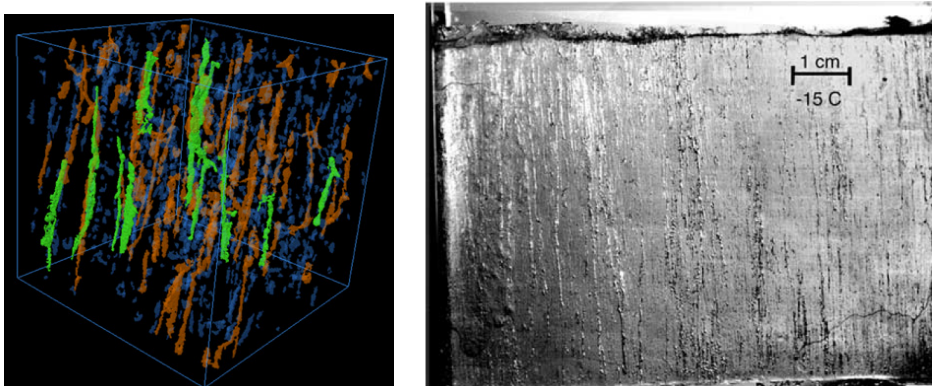
FIG. 3. *Vertical pores and smaller vertically aligned inclusions in first-year sea ice. (Left) Sea ice at* $-20\,^{\circ}C$*, scanned via x-ray microcomputed tomography. Edge of each side of cube is* 7.5 *mm. Color coding indicates channel volume; green* > 0.0337 *mm*^{3}*, blue* < 0.0067 *mm*^{3}*, and orange is intermediate* [18]. *(Right) A photograph of a vertical thick section cut from naturally grown first-year ice cut at a depth of approximately* 80 *cm (From* [19]*; reprinted with permission from John Wiley and Sons).*

the system. The Stefan-type problem is further simplified through a quasi-steady reduction to a mean curvature flow driven by the thermal gradient. This reduction aligns with recent work in the sea-ice community advocating for "the removal of the widely adopted planar-equilibrium representation of the surface tension, the so-called capillary approximation, in favor of consideration of the curvature or size-dependence of the surface tension" [13].

We calibrate the parameters to experimental data and use numerical simulations to examine the role of temperature gradients on pinch-off and migration of brine inclusions. We find that typical winter temperature gradients can have a significant impact on the structure of brine inclusions, contributing to the break-up (pinch-off) of longer brine pores into smaller, more spherical inclusions. More significantly for albedo, thermal gradients may impact the size distribution of the smaller inclusions. As shown in Figure 7 a strong thermal gradient coupled with a large decrease in temperature may produce more uniformly sized inclusions after break-up, such as are visible in Figure 3. The same thermal gradient with a smaller shift in temperature, as occurs towards the bottom of the ice sheet, produces a pinch-off at one end of the inclusion, suggesting that continuation beyond the initial pinch-off will lead to the formation of a string of small inclusions. The thermal gradient also induces a downward migration towards the warmer ice-bottom. This effect is particularly pronounced for spherical inclusions whose constant curvature cannot balance the inhomogeneity of the thermal gradient. This may provide a mechanism for the desalinization of the top layer of ice with the onset of warmer weather as is seen in the second row of data in Figure 1. We investigate the contribution of the density stratification of salt within a pore to downward migration but find that this effect is several orders of magnitude smaller.

There are important elements of sea ice that the model presented here does not capture. It does not include air bubbles, and it takes liquid water and ice to have the same density, ignoring expansion and the associated elastic effects induced by freezing. Sea ice is composed of a variety of salts, in particular mirabilite (Na_2SO_4) which begins to precipitate from solution at $-8.2\,^{\circ}$C and accumulate in the bottom of larger brine inclusions, impacting their shape and evolution [19]. Several effects,

including convective mixing during freezing, generate microstructure in sea ice that can influence brine channel shape [3, 18]. Core samples from the top of an ice sheet are more likely to be frazil ice with a random grain orientation, while mid-depth ice is generally columnar, with a more vertical orientation of ice grains and ice near the seawater interface is often platelet ice, with a higher degree of lateral grain structure. Our model approach is best adapted to columnar ice.

In section 2 we derive the thermodynamically consistent flow, including the change of variables from temperature to internal energy, and the reformulation in terms of the more slowly varying salt density relative to liquid water. In section 3 we use multiscale analysis to pursue the sharp-interface limit, deriving the Stefan-type problem for the ice-water interface and resolving the missing boundary condition. In section 4 we present the quasi-steady reduction to a thermal gradient–driven curvature flow and examine the impact of the thermal gradient within the context of axisymmetric brine inclusions. Temperature is measured in Kelvin in sections 2 and 3, as required for discussions of thermal entropy which is singular at 0 K. In section 4 connections are made to experimental sea ice data, and it is natural to change to degrees Celsius so that comparisons are more natural.

2. Model derivation. We derive a thermodynamically consistent system for a mixture of water, ice, and salt within a cubical region $\Omega \subset \mathbb{R}^3$ subject to zero-flux boundary conditions. This is a closed system corresponding to a sample of ice at a fixed depth within an ice sheet. The evolution uniformly increases the system entropy while preserving the internal energy and the total salt.

The main variables are the phase function ϕ, the temperature θ, and the salt weight fraction N (for natrium). The phase function denotes the percentage of the water molecules that are in the liquid state, thus $\phi = 1$ is liquid, and $\phi = 0$ is fully frozen. We incorporate salt to the phase field models introduced by Penrose and Fife in [24] by following the GENERIC framework. In the work of Penrose and Fife, the authors present several models for the free energy, internal energy, and entropy of the temperature-dependent phase change. We pursue the simplest of these, for which the entropy is expressed as a spatial integral

$$\tilde{S}(\phi, \theta) = \int_\Omega \tilde{s}(\nabla\phi, \phi, \theta) \, d\tilde{x},$$

over dimensional $\tilde{x}$ of an entropy density in the form

(2.1) $$\tilde{s}(\nabla\phi, \phi, \theta) = \nu(\phi)y(\theta, \phi) - e_0 W_0(\phi) - \sigma_\phi |\nabla\phi|^2.$$

Here W_0 is a classic double well potential with equal depth minima at $\phi = 0, 1$, and e_0 and σ_ϕ are constants. While this formulation has some deficiencies, including a nonconvex dependency of entropy on the phase field variable, they show that it connects directly to the classical phase field model, and it significantly simplifies the subsequent analysis. We modify this form of $\tilde{s}$ in several ways. First we incorporate salt dependence into the first term of $\tilde{s}$ in the form

$$\nu(\phi)y(\theta, \phi, N) = -e_1 W_1(\phi)\xi(\theta, N).$$

The potential W_1 is dimensionless and has $\phi = 0, 1$ as critical points so that

$$\tilde{W}(\phi; \theta, N) := e_0 W_0(\phi) + e_1 W_1(\phi)\xi(\theta, N)$$

is an unequal depth double well with respect to ϕ with local minima at $\phi = 0, 1$. Generic choices are

$$W_0(\phi) = 18\phi^2(1-\phi)^2,$$

(2.2)
$$W_1(\phi) = 2\phi^2\left(\phi - \frac{3}{2}\right).$$

The cryoscopic term ξ serves to raise or lower the value of the minima at $\phi = 1$. For small deviations of temperature and low salt concentrations the cryoscopic term is well approximated by a linear relation

(2.3)
$$\xi(\theta, N) := N + \beta(\theta - \theta_*),$$

where $\theta_* = 273$ K is the freezing point of pure water and $\beta = 1.85/\text{K}$; see Figure 2 and [29]. Since $\tilde{W}(0; \theta, N) = 0$, the sign of $\tilde{W}(1; \theta, N)$ encodes the entropic preference of the mixture for ice or liquid. We take $W_1 \leq 0$ on $[0,1]$, with the normalization $W_1(1) = -1$, so that positive values of ξ promote melting. The normalization of W_0 simplifies the scaling of the surface tension; see (3.7).

Two more modifications to $\tilde{s}$ incorporate temperature and salt dependence on system entropy. The first of these takes the simplest choice for the thermal entropy (see [20, page 238]):

(2.4)
$$\tilde{\Upsilon}(\theta) = e_s \ln \theta.$$

The thermal entropy coefficient is the product of specific heat c_s and density ρ_0,

$$e_s = c_s \rho_0 = (2072 \, \text{J kg}^{-1}\text{K}^{-1})(1000 \, \text{kg/m}^3) = 2.072 \times 10^6 \, \text{J K}^{-1}\text{m}^{-3}.$$

The specific heat is taken independent of phase [8, page 204]. While temperature is dimensional here, the inclusion of a dimensional scaling merely adds a constant to the system entropy and is avoided for simplicity of presentation.

The second and most significant modification to $\tilde{s}$ incorporates the entropy of the salt *relative to the molar density of liquid* water. The water molecules in the liquid state solvate the salt ions. Consequently the salt entropy decreases with the ratio of salt molecules to liquid-state water molecules. This decrease in entropy drives the chemotactic ejection of salt from freezing water. Density-driven stratification of salt within water is incorporated through a gravitational potential term

(2.5)
$$\tilde{\mathcal{R}}(\phi, N, \tilde{x}) = e_N N \left(1 - \ln \frac{N}{\phi}\right) - e_g N \tilde{x}_3/L_b,$$

where $L_b = 10^{-3} m$ is a typical brine length scale and $\tilde{x}_3$ is the component of $\tilde{x}$ along the direction of the gravitational force. The entropy of NaCl salt in water (at 20 °C) is roughly 43.4 $\text{J K}^{-1}\text{mol}^{-1}$ [15] while the molar density of water is $m_0 = 5.55 \times 10^4$ mol/m^3. This suggests an entropy coefficient

$$e_N = (43.4 \, \text{J K}^{-1}\, \text{mol}^{-1})\, m_0 = 2.41 \times 10^6 \, \text{J K}^{-1}\text{m}^{-3}.$$

The coefficient e_g quantifies the buoyancy gradient that salt induces in water, with gravity driving a salinity gradient at equilibrium. Water with N percent salt by weight has density $\rho_0(1 + 0.83N)$ where ρ_0 is density of pure water [4]. This gives a buoyant density of the salt water of $\rho_0 0.83N$ with units of kg/m^3. Introducing the gravitational acceleration $g = 9.8$ m/s^2 we have

$$e_g := 0.83\frac{g\rho_0 L_b}{\theta_*} = 2.98 \times 10^{-2} \, \text{J K}^{-1}\text{m}^{-3}.$$

Here $\theta_* = 273$ K is the reference temperature for arctic salt water. The dimensionless ratio of salt entropy to its buoyant counterpart, akin to a Grashof number for thermal gradients, takes the value

$$\delta_g := \frac{e_g}{e_N} = \frac{29.8 \times 10^{-3}}{2.41 \times 10^6} = 1.23 \times 10^{-8}.$$

The constant e_1 scales the latent heat. For water, the latent heat of freezing is $3.34 \times 10^6 \, \text{J/kg}$, so that

$$e_1 = \frac{(3.34 \times 10^6 \, \text{J kg}^{-1})\rho_0}{\theta_*} = 1.2 \times 10^7 \, \text{J K}^{-1}\text{m}^{-3}.$$

It is more difficult to estimate σ_ϕ and e_0; however, in the sharp interface regime the interfacial width satisfies $L_{li} = \sqrt{e_0/\sigma_\phi}$. For a liquid-ice water interface this width is $L_{li} = 10^{-9}$m [12]. We scale $\tilde{x}$ by the brine inclusion length $L_b = 10^{-3}m$, introducing the dimensionless length $x = \tilde{x}/L_b$, and correspondingly define $H := L_b/L_{li} \sim 10^6 \gg 1$, which serves as the large parameter in our analysis. Nondimensionalizing the system entropy by $e_s L_b^3$, we consider the classical sharp-interface scaling, imposing

$$
\begin{aligned}
(2.6) \qquad &\sigma_\phi = e_s L_{li}^2 H, \\
&e_0 = e_s H.
\end{aligned}
$$

For simplicity of notation we set $e_N = e_1 = e_s$. Shifting to dimensionless length and dropping the tilde notation, the system entropy takes the form

$$(2.7) \qquad S(\phi, \theta, N) = \int_\Omega \overbrace{\Upsilon(\theta) + \mathcal{R}(\phi, N, x) - \frac{1}{2H}|\nabla\phi|^2 - HW(\phi;\xi)}^{s(\nabla\phi,\phi,\theta,N)} \, dx.$$

The scaled potential takes the form

$$(2.8) \qquad W(\phi;\theta,N) = W_0(\phi) + \frac{1}{H}W_1(\phi)\xi(\theta,N),$$

while the thermal entropy

$$(2.9) \qquad \Upsilon(\theta) = \ln\theta$$

and salt entropy relative to liquid water

$$(2.10) \qquad \mathcal{R}(\phi,N,x) = N\left(1 - \ln\frac{N}{\phi}\right) - \delta_g N x_3$$

are dimensionless. We remark that time, measured in seconds, and temperature, measured in Kelvin, retain units. We avoid the notation required to scale the temperature since that serves only to modify the value and units of β and to shift the system entropy $\mathcal{S}$ by an additive constant that does not impact the system evolution.

2.1. The entropic gradient flow. We apply the thermodynamic framework as presented in [20] to develop a gradient flow that conserves the internal energy, increases the entropy, and conserves the total salt density. This requires replacing temperature with internal energy as a dependent variable. More specifically, the formulation to this point is in terms of the three dependent variables (ϕ, θ, N). To arrive at a flow

that conserves the internal energy u we determine the relation $\theta = \hat{\theta}(u, \phi)$ and convert to system in terms (ϕ, u, N) with $\theta = \hat{\theta}$ slaved.

Assuming smoothness, the Legendre transform allows us to express the free energy density ψ and internal energy density u though the entropic density s. When written in the form $\psi = \psi(\phi, \theta, N)$ the entropy satisfies

$$(2.11) \qquad\qquad s = -\partial_\theta \psi,$$

while the internal energy satisfies

$$(2.12) \qquad\qquad u = \psi - \theta \partial_\theta \psi = \psi + \theta s.$$

To determine ψ we integrate s from (2.7) with respect to θ. Neglecting any terms that are independent of θ yields

$$(2.13) \qquad \psi(\phi, \theta, N) = \frac{\theta}{2H}|\nabla\phi|^2 + \theta(HW_0(\phi) + NW_1(\phi)) + \frac{\beta(\theta - \theta_*)^2}{2}W_1(\phi)$$
$$- \overline{\Upsilon}(\theta) - \theta\mathcal{R}(\phi, N, x).$$

Here $\overline{\Upsilon}$ is the primitive of Υ with respect to θ. The volume integral of the free energy density is a conserved quantity—its gradients do not drive the flow. In this framework its significance is as an intermediate that determines the internal energy. From (2.12) this latter takes the form

$$(2.14) \qquad\qquad u = -\frac{\beta}{2}(\theta^2 - \theta_*^2)W_1(\phi) - \overline{\Upsilon}(\theta) + \theta\Upsilon(\theta).$$

In the case at hand $\overline{\Upsilon}(\theta) = \theta\Upsilon(\theta) - \theta$, and we can recast the internal energy as

$$(2.15) \qquad\qquad u = \theta - b(\theta)W_1(\phi),$$

where we have introduced

$$(2.16) \qquad\qquad b(\theta) := \frac{\beta}{2}(\theta^2 - \theta_*^2).$$

Within this formulation the internal energy and entropy densities satisfy the fundamental thermodynamic relation

$$(2.17) \qquad\qquad \frac{\partial_\theta u}{\partial_\theta s} = \frac{1 - \beta\theta W_1(\phi)}{\theta^{-1} - \beta W_1(\phi)} = \theta.$$

Subject to no-flux boundary conditions the thermodynamic evolution equations should increase the entropy density in space, while conserving the total internal energy

$$(2.18) \qquad\qquad E_T := \int_\Omega u(x)\,\mathrm{d}x$$

and the total salt amount

$$(2.19) \qquad\qquad N_T := \int_\Omega N(x)\,\mathrm{d}x.$$

This requires rewriting the evolution in terms of the internal energy and using (ϕ, u, N) as dependent variables. To this end we invert the relation (2.15), writing

$$(2.20) \qquad \hat{\theta} := \hat{\theta}(u, \phi).$$

This inverse is well defined and smooth in the regime we consider. The entropy takes the form

$$(2.21) \qquad \hat{S}(\phi, N, u) = \int_{\Omega} \Upsilon(\hat{\theta}(u, \phi)) + \mathcal{R}(\phi, N, x) - \frac{1}{2H}|\nabla\phi|^2 - HW(\phi; \hat{\xi}) \, dx,$$

where, to emphasize that the cryoscopic relation has become a function of u and ϕ, we introduce

$$(2.22) \qquad \hat{\xi}(\phi, u, N) := N + \beta(\hat{\theta}(\phi, u) - \theta_*).$$

The flow is determined by the gradient of $\hat{S}$, through a choice of dissipation mechanism. The mass of ice and water are not individually conserved. This motivates a choice of nonconservative gradient for the liquid phase function

$$(2.23) \qquad \phi_t = \frac{\delta\hat{S}}{\delta\phi},$$

where

$$(2.24) \qquad \frac{\delta\hat{S}}{\delta\phi} = \frac{1}{H}\Delta\phi - HW'(\phi, \hat{\xi}) + \left(\Upsilon'(\hat{\theta}) - \beta W_1(\phi)\right)\partial_\phi\hat{\theta} + \partial_\phi\mathcal{R}(\phi, N, x).$$

Here prime denotes differentiation with respect to the function's first variable. Taking ∂_ϕ of (2.15) we calculate that

$$(2.25) \qquad \partial_\phi\hat{\theta} = \frac{b(\theta)W_1'(\phi)}{1 - \beta\hat{\theta}W_1(\phi)}.$$

Since $\Upsilon' = \theta^{-1}$ we find that the phase field equation for ϕ reduces to

$$(2.26) \qquad \phi_t = \frac{1}{H}\Delta\phi - HW_0'(\phi) - W_1'(\phi)\left(N + b(\hat{\theta})/\hat{\theta}\right) + \partial_\phi\mathcal{R}(\phi, N, x),$$

where $b(\theta)/\theta$, in increasing function of θ.

For zero-flux boundary conditions the total internal energy is conserved by the flow

$$(2.27) \qquad u_t = -\nabla \cdot \left(M_u\nabla\frac{\delta\hat{S}}{\delta u}\right),$$

where from (2.21)

$$(2.28) \qquad \frac{\delta\hat{S}}{\delta u} = \left(\hat{\theta}^{-1} - \beta W_1(\phi)\right)\partial_u\hat{\theta}(u, \phi).$$

Taking ∂_u of (2.15) we derive

$$(2.29) \qquad \partial_u\hat{\theta} = \frac{1}{1 - \beta\hat{\theta}W_1(\phi)},$$

and hence, as is consistent with (2.17), we obtain

$$(2.30) \qquad \frac{\delta\hat{S}}{\delta u} = \hat{\theta}^{-1}.$$

For the canonical choice, $M_u = \sigma_\theta\hat{\theta}^2$, (see [24, page 50]), we derive the relation

$$(2.31) \qquad u_t = \sigma_\theta\Delta\hat{\theta},$$

where σ_θ is the thermal conductivity, taken for simplicity to be independent of phase. The salt flux is generated by the entropy through the mass preserving flow

$$(2.32) \qquad N_t = -\nabla \cdot \left(M_N \nabla \frac{\delta \hat{S}}{\delta N} \right),$$

where the variation of $\hat{S}$ with respect to N is given by

$$(2.33) \qquad \frac{\delta \hat{S}}{\delta N} = -W_1(\phi)\partial_N \hat{\xi} + \partial_N R(\phi, N, x)$$

$$(2.34) \qquad = -W_1(\phi) - \ln\left(\frac{N}{\phi}\right) - \delta_g x_3.$$

Taking $M_N = \sigma_N N$, where σ_N is a constant, we obtain

$$(2.35) \qquad N_t = \sigma_N \nabla \cdot \left(N\nabla \left(W_1(\phi) + \ln\frac{N}{\phi} + \delta_g x_3 \right) \right)$$

$$(2.36) \qquad = \sigma_N \nabla \cdot \left(N\left(W_1'(\phi) - \frac{1}{\phi} \right)\nabla\phi + \nabla N + \delta_g \mathbf{e}_3 N \right).$$

To summarize, the coupled system takes the form

$$(2.37) \qquad \phi_t = \frac{1}{H}\Delta\phi - HW_0'(\phi) - W_1'(\phi)\left(N + b(\hat{\theta})/\hat{\theta} \right) + \frac{N}{\phi},$$

$$(2.38) \qquad u_t = \sigma_\theta \Delta\hat{\theta},$$

$$(2.39) \qquad N_t = \sigma_N \nabla \cdot \left(N\left(W_1'(\phi) - \frac{1}{\phi} \right)\nabla\phi + \nabla N + \delta_g \mathbf{e}_3 N \right).$$

The advantage of this framework is that, subject to zero-flux boundary conditions, the system enjoys an entropy generation mechanism

$$(2.40) \qquad \frac{d\hat{S}}{dt} = \int_\Omega \left| \frac{\delta \hat{S}}{\delta \phi} \right|^2 + M_u \left| \nabla\frac{\delta \hat{S}}{\delta u} \right|^2 + M_N \left| \nabla\frac{\delta \hat{S}}{\delta N} \right|^2 \, \mathrm{d}x \geq 0,$$

whose density is pointwise positive throughout the domain. In this sense the system satisfies the Clausius–Duhem (or second law) inequality, while maintaining conservation of total internal energy and salt.

2.2. Relative salt density and model reformulation. With the system (2.35)–(2.39) defined through the variational formulation, we are now free to change to variables that simplify the subsequent multiscale analysis of section 3. We remove the fast variation from the salt variable and replace the internal energy with the temperature as a dependent variable. The salt flux is given by

$$(2.41) \qquad J_N := N\sigma_N \left(\nabla\left(W_1 + \ln\frac{N}{\phi} \right) + \delta_g \mathbf{e}_3 \right).$$

Setting aside the small gravitational term, the equilibrium with zero salt-flux have salt distributions of the form

$$(2.42) \qquad N = \rho\phi e^{-W_1(\phi)},$$

where $\rho > 0$ is a spatial constant defining the salt density *relative* to liquid water density. This suggests that θ and ρ can be viewed as slowly varying quantities, and we change to the variables (ϕ, θ, ρ) from (ϕ, u, N). A key step is the introduction of the modified potential

$$(2.43) \qquad V(\phi; \theta, \rho) = W_0(\phi) + \frac{1}{H} V_1(\phi; \theta, \rho),$$

where the modified perturbation to the double well

$$
\begin{aligned}
(2.44) \qquad V_1(\phi; \theta, \rho) &:= \int_0^\phi \left(b(\theta)/\theta + \rho s e^{-W_1(s)} \right) W_1'(s) - \rho e^{-W_1(s)} \, ds \\
&= W_1(\phi) b(\theta)/\theta + \rho \left(\int_0^\phi -s \left(e^{-W_1(s)} \right)' - e^{-W_1(s)} \, ds \right) \\
&= W_1(\phi) b(\theta)/\theta - \rho \phi e^{-W_1(\phi)}.
\end{aligned}
$$

This perturbation breaks the equal-depth structure; however, unlike W_1, it incorporates influence from the salt entropy, so that its value in the right well of W_0 is always negative. More specifically $V_1(0; \theta, \rho) = 0$ while

$$(2.45) \qquad V_1(1; \theta, \rho) = W_1(1) b(\theta)/\theta - \rho e^{-W_1(1)} = -b(\Theta)/\Theta - \rho e^1 < 0.$$

This shift in notation allows us to recast the system as

$$(2.46) \qquad \partial_t \phi = \frac{1}{H} \Delta \phi - H \partial_\phi V(\phi; \theta, \rho),$$

$$(2.47) \qquad \partial_t \left(\theta - b(\theta) W_1(\phi) \right) = \sigma_\theta \Delta \theta,$$

$$(2.48) \qquad \partial_t \left(\phi e^{-W_1(\phi)} \rho \right) = \sigma_N \nabla \cdot \left(\phi e^{-W_1(\phi)} \left(\nabla \rho + \delta_g \mathbf{e}_3 \rho \right) \right).$$

The product of W_1 and the function $b(\theta)$, defined in (2.16), provides the form and scaling for the latent heat. In this formulation the salt exclusion mechanism is incorporated into the time derivative term on the left-hand side of (2.48).

Table of Parameters

Symbol	Description	Value	Units
ρ_0	Water density	1000	kg/m^3
c_s	Specific heat of ice at $-5\,^\circ$C	2072	J/(K kg)
S_e	NaCl salt in water molar entropy	43.4	J/(K mol)
m_0	Water molar density	5.55×10^4	mol/m^3
g	Gravitational acceleration	9.8	m/s^2
θ_*	Reference temperature	273	K
β	Cryoscopic parameter	1.85	1/K
e_s	Thermal entropy coefficient	2.5×10^6	J/(K m^3)
e_N	Salt entropy coefficient	2.41×10^6	J/(K m^3)
e_g	Gravitational entropy coefficient	2.98×10^{-2}	J/(K m^3)
e_1	Latent heat coefficient	1.2×10^7	J/(K m^3)
L_b	Brine inclusion length scale	10^{-3}	m
L_{li}	Liquid-ice interface length scale	10^{-9}	m
δ_g	Density stratification ratio	1.23×10^{-8}	-
H	Ratio of inclusion lengths to interface	10^6	-

3. Reduction to a Stefan-type problem. In the sharp-interface limit, $H \gg 1$, we use multiscale asymptotics to derive a Stefan-type problem for the evolution of the ice-liquid interface $\Gamma = \Gamma(t)$. The salt rejection mechanism leads to a nonsmooth
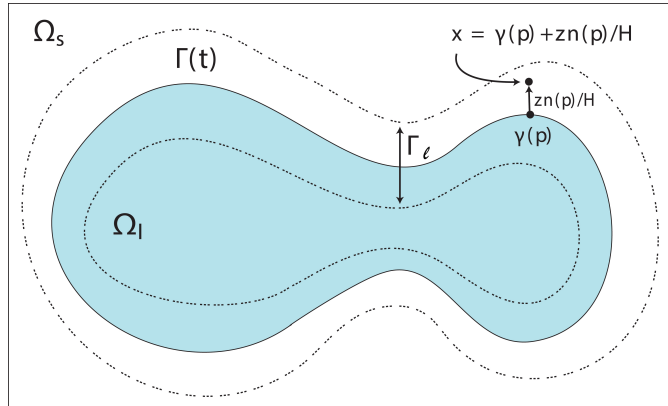
FIG. 4. *Partition of domain Ω into the disjoint outer regions Ω_s (white—solid ice) and Ω_l (blue—liquid), separated by the moving interface $\Gamma(t)$. The inner region Γ_ℓ contains Γ, is bounded by the dotted lines, partially overlaps the outer regions, and supports the Frenet coordinate system (3.1).*

variation in the the absolute quantity of salt, s, across the interface, but the relative salt, ρ, remains smooth. The outer problem derived that results from matched asymptotics is underdetermined, and we obtain a closed system by imposing conservation of salt under local interface variation.

We consider a brine inclusion whose boundary is given by a smooth, closed 2-dimensional manifold Γ immersed in $\Omega \subset \mathbb{R}^3$; see Figure 4. We define the local Frenet coordinates system in a neighborhood of Γ via the mapping

$$(3.1) \qquad x = \zeta(p, z) := \gamma(p) + H^{-1}\mathbf{n}(p)z,$$

where $\gamma : \mathcal{P} \to \mathbb{R}^3$ is a local parameterization of Γ and $\mathbf{n}$ is the outward unit normal to Γ. The variables $p = (p_1, p_2)$ parameterize the tangential directions of Γ while z denotes the H-scaled, signed distance to Γ, negative in the liquid region Ω_l and positive on the solid region Ω_s.

In a neighborhood Γ_ℓ of $\Gamma = \Gamma(t)$

$$(3.2) \qquad \Gamma_\ell := \left\{ \zeta(p, z) \in \mathbb{R}^3 \ \middle|\ p \in \mathcal{P}, \ -\ell H \leq z \leq \ell H \right\} \subset \Omega,$$

the Cartesian gradient and Cartesian Laplacian admit the formulation

$$(3.3) \qquad \nabla_x = H\mathbf{n}\partial_z + \nabla_p,$$

$$(3.4) \qquad \Delta_x = H^2\partial_z^2 + H\kappa_0(p)\partial_z + (z\kappa_1(p)\partial_z + \Delta_p) + O(H^{-1}).$$

Here κ_i is a sum of the $(i+1)$st powers of the two curvatures $\{K_1, K_2\}$ of Γ,

$$\kappa_i := (-1)^i \sum_{j=1}^{2} K_j^{i+1}.$$

In particular, κ_0 is the sum of the curvatures and is often called the total curvature of Γ. With this choice of normal the curvature of a sphere is negative [17]. The interface Γ evolves in time through its normal velocity

$$(3.5) \qquad \mathrm{V_n}(p, t) := -H^{-1}\dot{z},$$

where $\dot{z} := \frac{\partial z}{\partial t}$ gives the rate of approach of the front to a point $x = x(z, p)$. It admits an expansion of the form

$$(3.6) \qquad \dot{z} = \dot{z}_0 + H^{-1}\dot{z}_1 + O(H^{-2}).$$

3.1. Expansions and matching conditions. The front profile $\tilde{\Phi}_0$ is defined to be the solution of the equation

$$(3.7) \qquad \partial_z^2 \tilde{\Phi}_0 = W_0'(\tilde{\Phi}_0),$$

which satisfies $\tilde{\Phi}_0 \to \tilde{\Phi}_0^{\pm}$ as $z \to \pm\infty$, where $\tilde{\Phi}_0^{+} = 0$ and $\tilde{\Phi}_0^{-} = 1$ are the two minima of W_0. The linear operator obtained by linearizing (3.7) about $\tilde{\Phi}_0$ is denoted

$$(3.8) \qquad \mathrm{L} := \partial_z^2 - W_0''(\tilde{\Phi}_0).$$

The function $\Phi_0 \in H^2(\Omega)$ relates to $\tilde{\Phi}_0$ through the relation $\Phi_0(x) = \tilde{\Phi}_0(z(x))$ on Γ_ℓ and is extended smoothly to take values $\tilde{\Phi}_0^{\pm}$ off of Γ_ℓ. We consider a formal, multiscale analysis of the temperature θ, molar salinity ρ, and the phase parameter ϕ. In the far-field, away from the interface Γ, $\rho = N$, and the system admits the outer expansion

$$(3.9) \qquad \theta = \Theta_0(x, t) + H^{-1}\Theta_1(x, t) + O(H^{-2}),$$

$$(3.10) \qquad \phi = \Phi_0(x, t) + H^{-1}\Phi_1(x, t) + O(H^{-2}),$$

$$(3.11) \qquad N = N_0(x, t) + H^{-1}N_1(x, t) + O(H^{-2}).$$

To avoid fast transients we consider a "relaxed" regime in which the phase change is equilibrated at leading order in the outer region. In the outer region, that is, off of Γ_ℓ, the leading order front profile Φ_0 is piecewise constant. This motivates the introduction of the liquid region $\Omega_s(t) = \{x \,|\, \Phi_0(x, t) = 1\}$ and the complementary solid region $\Omega_s(t) = \{x \,|\, \Phi_0(x, t) = 0\}$. We use χ_l the indicator of the liquid domain Ω_l to express Φ_0, i.e.,

$$\Phi_0(x, t) = \chi_l(x, t) = \begin{cases} 1 & \text{if } x \in \Omega_l, \\ 0 & \text{if } x \in \Omega_s. \end{cases}$$

While the interface moves in time, this is reflected in the outer region only through the matching conditions.

To simplify notation, we introduce the outer vector $\mathbf{U} = [\Theta, N]^t$ and its expansion

$$(3.12) \qquad \mathbf{U} = \sum_{i \geq 0} H^{-i}\mathbf{U}_i, \quad \text{where} \quad \mathbf{U}_i = [\Theta_i, N_i]^t.$$

We assume that the inner variables admit expansions of the form

$$(3.13) \qquad \theta(x, t) = \tilde{\theta}(z, p, t) = \tilde{\theta}_0(z, p, t) + H^{-1}\tilde{\theta}_1(z, p, t) + O(H^{-2}),$$

$$(3.14) \qquad \phi(x, t) = \tilde{\phi}(z, p, t) = \tilde{\Phi}_0(z) + H^{-1}\tilde{\phi}_1(z, p, t) + O(H^{-2}),$$

$$(3.15) \qquad \rho(x, t) = \tilde{\rho}(z, p, t) = \tilde{\rho}_0(z, p, t) + H^{-1}\tilde{\rho}_1(z, p, t) + O(H^{-2}).$$

At the interface we have matching conditions for both the temperature and the salinity. The temperature satisfies the matching condition

$$(3.16) \qquad \lim_{h \to 0} \Theta(x + h\mathbf{n}, t) = \lim_{z \to \pm\infty} \tilde{\theta}(z, p, t),$$

which for $x \in \Gamma$ yields the relations

$$(3.17) \qquad \Theta_0^\pm(x,t) = \lim_{z \to \pm\infty} \tilde{\theta}_0(z,p,t),$$

$$(3.18) \qquad \Theta_1^\pm(x,t) + z\partial_{\mathbf{n}}\Theta_0^\pm(x,t) = \lim_{z \to \pm\infty} \tilde{\theta}_1(z,p,t).$$

Here $\mathbf{n}$ is the outward unit normal to Γ, $\partial_{\mathbf{n}}$ is the derivative in the normal direction of Γ, and $\Theta_i^\pm$ denote the values of the limits of the left-hand side in (3.16) as $h \to 0$, respectively.

The matching conditions on the salinity incorporate the relation $N = \rho\phi e^{-W_1(\phi)}$ and the usual limiting behavior,

$$(3.19) \qquad \lim_{h \to 0} N(x + h\mathbf{n}, t) = \lim_{z \to \pm\infty} \tilde{\rho}(z,p,t)\tilde{\phi}(z,t,p)e^{-W_1(\tilde{\phi}(z,p,t))},$$

which for $x \in \Gamma$ yields the relations

$$(3.20) \qquad N_0^\pm(x,t) = \lim_{z \to \pm\infty} \tilde{\rho}_0(z,p,t)\tilde{\Phi}_0 e^{-W_1(\tilde{\Phi}_0)},$$

$$(3.21) \qquad N_1^\pm + z\partial_{\mathbf{n}}N_0^\pm = \lim_{z \to \pm\infty} \left[\tilde{\Phi}_0 e^{-W_1(\tilde{\Phi}_0)}(\tilde{\rho}_1 - \tilde{\rho}_0 W_1'(\tilde{\Phi}_0)\tilde{\phi}_1) + \tilde{\phi}_1\tilde{\rho}_0 e^{-W_1(\tilde{\Phi}_0)} \right].$$

3.2. The outer system. We use the outer expansion (3.9)–(3.11) to break the system (2.46)–(2.48) into orders of H. In the "relaxed" outer regime, $\Phi_0 = \chi_l$ for $x \in \Omega_s \cup \Omega_l$, and as a consequence the $O(H)$ system is trivially satisfied. The $O(1)$ equations take the form

$$(3.22) \qquad W_0''(\chi_l)\Phi_1 = -\partial_\phi V_1(\chi_l; \mathbf{U}_0),$$

$$(3.23) \qquad \partial_t(\Theta_0 - b(\Theta_0)W_1(\chi_l)) = \sigma_\theta \Delta\Theta_0,$$

$$(3.24) \qquad \partial_t N_0 = \sigma_N \nabla \cdot (\nabla N_0 + \delta_g \mathbf{e}_3 N_0).$$

Since $W_1(0) = 0$ and $W_1'(\chi_l) = 0$, the derivatives of the modified potential V_1 (2.44) satisfy the relations

$$(3.25) \qquad \partial_\phi V_1(0; \mathbf{U}_0) = -\rho_0, \qquad \partial_\phi V_1(1; \mathbf{U}_0) = -\rho_0 e^{-W_1(1)}.$$

From the normalization $W_1(1) = -1$ we have $W_1(\chi_l) = -\chi_l$, and the $O(1)$ system can be written in terms of χ_l over the entire outer region as

$$(3.26) \qquad \Phi_1 = \frac{\rho_0 e^{\chi_l}}{W_0''(\chi_l)} \qquad\qquad \text{in } \Omega/\Gamma,$$

$$(3.27) \qquad (1 + b(\Theta_0)\chi_l)\partial_t\Theta_0 = \sigma_\theta \Delta\Theta_0,$$

$$(3.28) \qquad \partial_t N_0 = \sigma_N \nabla \cdot (\nabla N_0 + \delta_g \mathbf{e}_3 N_0) \qquad \text{in } \Omega/\Gamma.$$

This system is subject to interior layer matching and exterior boundary conditions derived in what follows. The phase parameter is zero in the ice region, and it is constant with a small perturbation which depends upon the salinity in the liquid region

$$(3.29) \qquad \phi(x,t) = 1 + H^{-1}\frac{\rho_0 e^{-W_1(1)}}{W_0''(1)} + O(H^{-2}).$$

3.3. The inner system. In the inner region we combine the system (2.46)–(2.48), the variable expansions (3.13)–(3.15), and the gradient and the Laplacian expansions (3.3)–(3.4). Collecting terms in orders of H we find at $O(H^2)$

$$(3.30) \qquad 0 = \partial_z^2 \tilde{\theta}_0 \qquad \qquad \text{in } \Gamma_\ell,$$

$$(3.31) \qquad 0 = \partial_z(\tilde{\Phi}_0 e^{-W_1(\tilde{\Phi}_0)} \partial_z \tilde{\rho}_0) \qquad \qquad \text{in } \Gamma_\ell.$$

Equation (3.30) implies that $\tilde{\theta}_0$ is linear in z. The matching condition (3.17) implies that $\tilde{\theta}_0$ is constant in z, which yields the continuity condition on the outer temperature,

$$(3.32) \qquad \qquad [\![\Theta_0]\!] = 0 \quad \text{on } \Gamma.$$

We conclude that $\tilde{\theta}_0 = \Theta_0$. At $O(H)$, the system takes the form

$$(3.33) \qquad 0 = \partial_z^2 \tilde{\Phi}_0 - W_0'(\tilde{\Phi}_0),$$

$$(3.34) \qquad 0 = \sigma_\theta \partial_z^2 \tilde{\theta}_1 + \kappa_0 \partial_z \tilde{\theta}_0,$$

$$(3.35) \qquad 0 = \partial_z(\tilde{\Phi}_0 e^{-W_1(\tilde{\Phi}_0)} \partial_z \tilde{\rho}_1)$$
$$+ \left(\kappa_0 \tilde{\Phi}_0 e^{-W_1(\tilde{\Phi}_0)} + \partial_z(\tilde{\phi}_1 e^{-W_1(\tilde{\Phi}_0)}(1 - W_1'(\tilde{\Phi}_0)\tilde{\Phi}_0)) \right) \partial_z \tilde{\rho}_0$$
$$+ \partial_z(\tilde{\Phi}_0 e^{-W_1(\tilde{\Phi}_0)}) \delta_g \tilde{\rho}_0 \mathbf{n} \cdot \mathbf{e}_3.$$

The equation (3.33) and matching conditions are consistent with the assumption that $\tilde{\Phi}_0$ provides the leading order inner expansion, in particular, that it is independent of the tangential variable p.

Since $\tilde{\theta}_0$ is independent of z, (3.34) implies that $\tilde{\theta}_1$ is linear in z and combined with the matching condition (3.18) yields the two interfacial zero-jump conditions for the outer temperature

$$(3.36) \qquad \qquad [\![\partial_\mathbf{n} \Theta_0]\!] = 0, \quad [\![\Theta_1]\!] = 0.$$

Addressing the $O(H^2)$ salt equation (3.31), we integrate twice with respect to z from 0 to z and solve for $\tilde{\rho}_0$. This yields the relation

$$(3.37) \qquad \tilde{\rho}_0(z, p, t) = \tilde{\rho}_0(0) + \left(\tilde{\Phi}_0(0) e^{-W_1(\tilde{\Phi}_0(0))} \partial_z \tilde{\rho}_0(0) \right) \int_0^z \frac{1}{\tilde{\Phi}_0(y) e^{-W_1(\tilde{\Phi}_0(y))}} \, dy,$$

where for brevity $\tilde{\rho}_0(0)$ is used here and below to denote $\tilde{\zeta}_0(0, p, t)$. Reporting this back to the matching condition (3.20), we have

$$(3.38) \qquad N_0^\pm(x, t) = \lim_{z \to \pm\infty} \tilde{\Phi}_0(z) e^{-W_1(\tilde{\Phi}_0(z))} \left[\tilde{\rho}_0(0) \right.$$
$$\left. + \left(\tilde{\Phi}_0(0) e^{-W_1(\tilde{\Phi}_0(0))} \partial_z \tilde{\rho}_0(0) \right) \int_0^z \frac{1}{\tilde{\Phi}_0(y) e^{-W_1(\tilde{\Phi}_0(y))}} \, dy \right].$$

As $z \to -\infty$, $\tilde{\Phi}_0 \to 1$ so that $W_1(\tilde{\Phi}_0(z)) \to W_1(1)$ and hence remains bounded. The dominant contribution comes from the term

$$(3.39) \qquad \lim_{z \to -\infty} e^{-W_1(\tilde{\Phi}_0(z))} \tilde{\Phi}_0(z) \int_0^z \frac{1}{e^{-W_1(\tilde{\Phi}_0(y))} \tilde{\Phi}_0(y)} \, dy = z + O(1).$$

The matching condition requires that $\partial_z \tilde{\rho}_0(0) = 0$, and hence $\tilde{\rho}_0$ is independent of z, and

$$
(3.40) \qquad N_0^- = \tilde{\rho}_0(0)e^{-W_1(1)} \qquad\qquad \text{on } \Gamma_\ell,
$$

$$
(3.41) \qquad N_0^+ = 0 \qquad\qquad \text{in } \Omega_s.
$$

With $\tilde{\rho}_0$ independent of z, the $O(H)$ salt equation (3.35) reduces to

$$
(3.42) \qquad \partial_z(\tilde{\Phi}_0 e^{-W_1(\tilde{\Phi}_0)}\partial_z\tilde{\rho}_1) = -\partial_z(\tilde{\Phi}_0 e^{-W_1(\tilde{\Phi}_0)})\delta_g\tilde{\rho}_0 \mathbf{n} \cdot \mathbf{e}_3.
$$

This has solutions of the form

$$
(3.43) \qquad \tilde{\rho}_1(z) = \tilde{\rho}_1(0) - z\delta_g\tilde{\rho}_0 \mathbf{n} \cdot \mathbf{e}_3 + \tilde{\Phi}_0(0)e^{-W_1(\tilde{\Phi}_0(0))}(\partial_z\tilde{\rho}_1(0)
$$
$$
+ \delta_g\tilde{\rho}_0 \mathbf{n} \cdot \mathbf{e}_3)\int_0^z \frac{1}{\tilde{\Phi}_0(y)e^{-W_1(\tilde{\Phi}_0(y))}}\,dy.
$$

We couple (3.43) with the matching condition (3.21). Since $\tilde{\phi}_1$ is uniformly bounded and $\tilde{\rho}_0$ is independent of z we use (3.39) to match terms in z as $z \to -\infty$, finding that

$$
(3.44) \qquad \partial_{\mathbf{n}}N_0^- = \tilde{\Phi}_0(0)e^{-W_1(\tilde{\Phi}_0(0))}\partial_z\tilde{\rho}_1(0).
$$

Conversely, as $z \to \infty$ we have $\tilde{\Phi}_0 \to \tilde{\Phi}_0^+ = 0$, for which $W_1(0) = 0$. Linearizing (3.33) about the limiting value $\tilde{\Phi}_0^+$ yields the equation

$$
\partial_z^2\tilde{\Phi}_0 - W''(\tilde{\Phi}_0^+)\tilde{\Phi}_0 = 0,
$$

which implies that $\tilde{\Phi}_0 = c_+ e^{-k_+ z}$ as $z \to \infty$, where $k_+ = \sqrt{W''(\tilde{\Phi}_0^+)}$. Using this asymptotic reduction, we have the relation

$$
(3.45) \qquad \lim_{z \to +\infty} \tilde{\Phi}_0(z,t)\int_0^z \frac{1}{\tilde{\Phi}_0(y,t)}\,dy = \frac{1}{k_+}.
$$

Using this limit in the matching condition we determine that

$$
(3.46) \qquad \partial_{\mathbf{n}}N_0^+ = 0,
$$

which is consistent with (3.41).

The function N_0 is discontinuous across the moving interface $\Gamma = \Gamma(t)$, and the interfacial conditions, expressed in terms of $\tilde{\rho}_0$ and $\partial_z\tilde{\rho}_1$, are underdetermined. We close the interfacial condition for N_0 by imposing local conservation of salt mass under interface deformation. Since $N_0 = 0$ in the ice domain Ω_s, conservation of mass requires that

$$
\partial_t \int_{\Omega_l} N_0\,dx = 0,
$$

which, using (3.28) and the normal velocity V_n, breaks into

$$
(3.47) \qquad 0 = \int_\Gamma N_0 V_\mathrm{n}\,ds + \int_{\Omega_l} \partial_t N_0\,dx
$$

$$
(3.48) \qquad = \int_\Gamma N_0 V_\mathrm{n}\,ds + \sigma_N^2 \int_{\Omega_l} \nabla \cdot (\nabla N_0 + \delta_g\mathbf{e}_3 N_0)\,dx
$$

$$
(3.49) \qquad = \int_\Gamma \left[N_0 V_\mathrm{n} + \sigma_N^2\left(\nabla N_0 + \delta_g N_0\mathbf{e}_3\right) \cdot \mathbf{n}\right]\,ds.
$$

Returning to the $\dot{z}$ formulation from (3.5), this implies the leading order boundary condition

$$(3.50) \qquad \frac{\dot{z}_0}{H} N_0 = \sigma_N^2 \left(\nabla N_0 + \delta_g N_0 \mathbf{e}_3 \right) \cdot \mathbf{n} \qquad\qquad \text{on } \Gamma.$$

We call this a sweeping boundary condition since the moving interface, reflected by $\dot{z}_0$, "sweeps up" the salt, a bit like a broom. More specifically, when the front motion is directed into the liquid domain, $\dot{z}_0 < 0$, the salt on the boundary is convected by the moving boundary to remain in the liquid domain so that at leading order no salt is left behind in the advancing ice region.

A closed system for the leading order outer variables requires an expression for the normal velocity. This arises from the O(1) equation for the phase field variable which takes the form

$$(3.51) \qquad \mathrm{L}\tilde{\phi}_1 = \dot{z}_0 \tilde{\Phi}_0' - \kappa_0 \tilde{\Phi}_0' - \partial_\phi V_1(\tilde{\Phi}_0; \mathbf{U}_0),$$

where the operator L is defined in (3.8). The solvability condition for (3.51) requires that the right-hand side be orthogonal to the kernel $\tilde{\Phi}_0'$ of L. Taking the inner product and solving for $\dot{z}_0$ yields the expression

$$(3.52) \qquad \dot{z}_0 = \kappa_0 + \frac{\langle \partial_\phi V_1(\tilde{\Phi}_0; \mathbf{U}_0), \tilde{\Phi}_0' \rangle}{\|\tilde{\Phi}_0'\|_{L^2}^2}.$$

Since $\mathbf{U}_0$ is constant in z it follows from (2.45) that

$$\left\langle \partial_\phi V_1(\tilde{\Phi}_0; \mathbf{U}_0), \tilde{\Phi}_0' \right\rangle = V_1(\phi; \mathbf{U}_0)\big|_{\phi=0}^{\phi=1} = W_1(1)b(\theta)/\theta - \rho e^{-W_1(1)} < 0.$$

With the matching condition (3.40) on N_0^- and the normalization $W_1(1) = -1$, the expression (3.52) yields the scaled normal velocity

$$(3.53) \qquad \dot{z}_0 = \kappa_0 - \|\Phi_0'\|_{L^2}^{-2} \left(b(\Theta_0)/\Theta_0 + N_0 \right) \qquad\qquad \text{on } \Gamma,$$

which couples temperature, salinity, and curvature. We summarize these results in section 4.

4. Stefan-type problem for brine inclusions in sea ice. A brine inclusion is defined by its evolving boundary $\Gamma = \Gamma(t)$, which divides the scaled region $\Omega = [0, d_0]^3$ into subdomains Ω_s and Ω_l. In the previous section we obtained a Stefan-type problem for the evolution of Γ in terms of the leading order outer variables. The salt N is zero on the exterior domain Ω_s and is discontinuous across the interface. It can be taken to be defined only on the interior domain, Ω_l. At leading order the phase equation is replaced by the location of the interface. We supplement the system with Dirichlet conditions on the temperature at the top $\partial\overline{\Omega} = [0, d_0]^2 \times \{d_0\}$ and the bottom $\partial\underline{\Omega} := [0, d_0]^2 \times \{0\}$, and zero-flux conditions on the lateral sides $\partial\Omega_s := \partial\Omega \backslash (\partial\overline{\Omega} \cup \partial\underline{\Omega})$. These inhomogenous Dirichlet boundary conditions reflect the temperature gradient that is a key feature of sea ice. However the system is not closed acted, the internal energy need not be globally conserved, and the global dissipation inequality (2.40) may not hold. Nonetheless the local analysis of section 3 remains valid. We study the slow evolution of the evolving boundary $\Gamma(t)$, in particular under the influence of the temperature gradient imposed through the boundary conditions Θ_b for Θ_0 at the top and bottom of Ω. The system reduces to a nonlinear parabolic equation for the temperature,

$$(4.1) \qquad (1 + b(\Theta_0)\chi_l)\partial_t \Theta_0 = \sigma_\theta \Delta \Theta_0, \qquad\qquad x \in \Omega,$$

$$(4.2) \qquad \Theta_0 = \Theta_b(x,t), \qquad\qquad \partial\overline{\Omega} \cup \partial\underline{\Omega},$$

$$(4.3) \qquad \partial_{\mathbf{n}}\Theta_0 = 0, \qquad\qquad x \in \partial\Omega_l,$$

where χ_l is the characteristic function for the inclusion region, and a parabolic equation for the salt on the evolving brine inclusion region of the form

$$(4.4) \qquad \partial_t N_0 = \sigma_N \nabla \cdot (\nabla N_0 + \delta_g \mathbf{e}_3 N_0), \qquad\qquad x \in \Omega_l,$$

$$(4.5) \qquad \partial_{\mathbf{n}} N_0 = 0, \qquad\qquad x \in (\partial\Omega) \cap \Omega_l.$$

The system is subject to the interfacial boundary condition which insures conservation of salt under the moving interface,

$$(4.6) \qquad \frac{\dot{z}_0}{H} N_0 = \sigma_N^2 \left(\nabla N_0 + \delta_g N_0 \mathbf{e}_3\right) \cdot \mathbf{n} \qquad\qquad \text{on } \Gamma.$$

Here the H-scaled signed distance z_0 to Γ satisfies

$$(4.7) \qquad \dot{z}_0 = \kappa_0 - \|\Phi_0'\|_{L^2}^{-2} \left(b(\Theta_0)/\Theta_0 + N_0\right) \qquad\qquad \text{on } \Gamma.$$

The system couples through the salt-preserving boundary condition (4.6) and the normal velocity (4.7). The coupling is at $O(H^{-1})$, the same formal order as the second-order outer system. However on the long $O(H)$ time scale both the leading and second-order systems relax to quasi-equilibrium, and the coupling between the second order and first order reduces to $O(H^{-2})$ and is negligible. The leading order temperature system is parabolic with nonlinearity arising only through the temperature and spatial dependence of the latent heat, $b(\theta)\chi_l$. Since $b > 0$, the system is uniformly parabolic in nondivergence form, and the parabolic regularity theory (see section 7.1 of [5]) applies. The salt weight fraction satisfies a scaled advection-diffusion equation within Ω_l and is defined to be zero outside this domain. The free boundary motion is also parabolic curvature driven flow with nonlinear forcing from the boundary values of the interior variables. The theory for the full system including coupling to the free boundary motion is not straightforward but we expect unique, regular solutions at least for short time and observe this in the computational simulations of the reduced model.

4.1. Quasi-equilibrium Stefan-type problem and its axisymmetric formulation. As can be seen from (4.6) on the fast t time scale the domain is constant to leading order, and both the heat and the salt equations satisfy unforced parabolic equations. Thus these quantities relax to quasi-equilibrium on this time-scale and are driven adiabatically by the interface which evolves on a slower $\tau = t/H$ time scale. In particular, for temperature boundary data that are spatially uniform on the top, $\partial\overline{\Omega}$, and the bottom, $\partial\underline{\Omega}$, the temperature relaxes to a simple linear equilibrium

$$(4.8) \qquad \Theta_0 = a_0 + b_0 x_3,$$

with $b_0 < 0$ reflecting that sea ice is generically warmer with increasing depth. Assuming that the brine inclusion region Ω_l does not intersect $\partial\Omega$, the salt density satisfies

$$(4.9) \qquad N_0 = N_T \frac{e^{-\delta_g x_3}}{\int_{\Omega_l} e^{-\delta_g x_3} \, dx}, \qquad\qquad x \in \Omega_l,$$

where the normalization incorporates the conservation of total salt, N_T.

The front evolution is driven quasi-adiabatically through the normal velocity. For simplicity we linearize $b(\Theta)/\Theta$, defined through (2.16), about $\Theta_0 = \theta_*$, consider the slow time scale, $\tau = t/H$, and observe that with the normalization (2.2) we have $\|\tilde{\Phi}_0'\|_{L^2} = 1$. With these adjustments the inner normal velocity $\tilde{V}_n = V_n/H$ takes the form

$$(4.10) \qquad \tilde{V}_n = -\kappa_0 + \xi(N_0, \Theta_0) = -\kappa_0 + N_0 + \beta(\Theta_0 - \theta_*).$$

The linearized normal velocity balances the cryoscopic term against curvature. Since $H \sim 10^6$, the slow time $\tau = 1$ corresponds to roughly two weeks, and $\tau = 5 - 10$ comprises a complete winter season.

With Θ_0 and N_0 prescribed as in (4.8)–(4.9), brine inclusions achieve shape equilibrium when the curvature balances the heat and salt gradients. Except for the temperature gradient, which is imposed, the problem for the equilibrium inclusion shape Γ uncouples from the full system. Given that brine inclusions are predominantly either spherical or vertically oriented tapered cylindrical pores, it is natural to consider a vertically oriented axisymmetric reduction for the curvature flow. In the next two sections we consider computations of this reduced problem in axisymmetric geometry, first steady state and then transient.

An axisymmetric surface of revolution has a parameterization

$$(4.11) \qquad \sigma(s, \mu) = (r(s) \cos \mu, r(s) \sin \mu, s)$$

over $[0, d] \times [0, 2\pi]$, where $r : [0, d] \mapsto \mathbb{R}$ denotes the radius of the surface measured from its vertical center line. The curvature is related to $r(s)$ through the equality

$$(4.12) \qquad \kappa_0 = -\frac{1 + (r')^2 - rr''}{2r\sqrt{(1 + (r')^2)^3}}.$$

More generally, under evolution by a normal velocity V_n the map $x_3 = x_3(s)$ becomes nontrivial, and the axisymmetric parameterization takes the form

$$\sigma(s, \mu) = (r(s) \cos \mu, r(s) \sin \mu, x_3(s)).$$

The outer normal to the interface is given by

$$\mathbf{n} = \frac{(x_3' \cos \mu, x_3' \sin \mu, -r')}{\sqrt{(x_3')^2 + (r')^2}},$$

while the time dependent r and x_3 parameterizations satisfy

$$(4.13) \qquad \begin{aligned} \partial_t r &= \frac{\tilde{V}_n x_3'}{\sqrt{(x_3')^2 + (r')^2}}, \\ \partial_t x_3 &= -\frac{\tilde{V}_n r'}{\sqrt{(x_3')^2 + (r')^2}}. \end{aligned}$$

The curvature satisfies

$$\kappa_0(s) = -\frac{(x_3')^3 + (r')^2 x_3' - rr'' x_3' + rr' x_3''}{2r\sqrt{((x_3')^2 + (r')^2)^3}},$$

where $'$ denotes ∂_s. The normal velocity is then computed in terms of s as

$$(4.14) \qquad \tilde{V}_n(s) = -\kappa_0(s) + N_0(x_3(s)) + \beta(\Theta_0(x_3(s)) - \theta_*).$$

Substituting (4.14) into (4.13) gives a closed evolution for $r(s, t)$ and $x_3(s, t)$ on the fixed domain $[0, d]$. Further details of the numerical approach and its convergence properties can be found in [22].
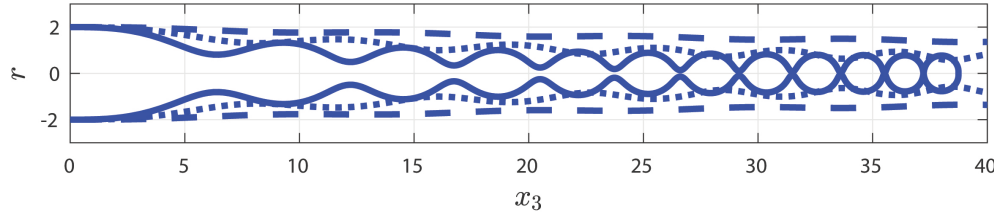
FIG. 5. *Cross-sections of axisymmetric equilibrium pore profiles obtained from* (4.15) *for* $x_3 > 0$. *The pores transition from slowly tapered to pinch-off for thermal gradients of* $1.5\,°C/m$ *(dashed),* $3.2\,°C/m$ *(dotted), and* $15.0\,°C/m$ *(solid). The simulation with the* $15.0\,°C/m$ *gradient terminates with a pinch-off singularity,* $r(x_3) = 0$, *at* $x_3 = 38.7$ *mm.*

4.2. Impact of thermal gradients on equilibrium pore structures. We neglect the minor role of density stratification, setting $\delta_g = 0$, so that N_0 is spatially constant over the inclusion, taking a value that depends only upon the volume of the inclusion and its total salt N_T. The steady-state version of the axisymmetric formulation shows the influence of thermal gradients on equilibrium pore shapes. Letting $r = r(x_3)$ denote the radius of an open-mouthed axisymmetric pore, then at equilibrium $V_n = 0$, and combining (4.10) and (4.12), the radius satisfies the second-order ODE

$$(4.15) \qquad -\frac{1 + (r')^2 - rr''}{2r\sqrt{(1 + (r')^2)^3}} = N_0 + \beta(\Theta_0(s) - \theta_*).$$

The salt-free freezing temperature is $\theta_* = 0\,°\text{C}$. The temperature profile Θ_0 depends on the depth as in (4.8) where a_0 denotes the temperature at the location $x_3 = 0$. The thermal gradient b_0 is constant in space, but it is taken at different seasonal values between 0.0015 and 0.015, corresponding to temperature gradients of $1.5\,°\text{C/m}$ to $15\,°\text{C/m}$. Smaller values of a_0 denote a deeper sample location within the ice.

We fix the local temperature a_0 and use Matlab ODE45 subroutine to resolve the system (4.15) with boundary data $r'(0) = 0$ and $r(0) = 2$ mm, corresponding to a large pore. The value of the constant salt density N is selected so that $r''(0) = 0$. This yields a spatially constant solution $r(x_3) = r(0)$ in the absence of a thermal gradient ($b_0 = 0$). Reintroducing the thermal gradient, we solve the system for $x_3 > 0$ corresponding to upwards towards the ice-air interface, the colder temperatures induce higher curvatures, and a smaller pore diameter. Figure 5 shows the progression of equilibrium pore cross-sections under thermal gradients of $1.5\,°\text{C/m}$, $3.2\,°\text{C/m}$, and $15\,°\text{C/m}$. The pore profile changes from weakly tapered to oscillatory with faster tapering at intermediate gradient to a pinch-off singularity at the largest gradient. While the oscillatory equilibrium and pinch-off states are surely unstable dynamically, they afford intuition to the role of thermal gradients in the system.

4.3. Impact of thermal gradients on inclusion evolution. The quasi-steady system (4.13)–(4.14) allows an investigation of the role of temperature gradients in the evolution of axisymmetric brine inclusions. These include both spherical and closed cylindrically axisymmetric inclusions. Spherical shapes are generically stable under curvature driven flows; indeed it is well known that motion by curvature produces spherical collapse states. In sea ice the salt concentration of a spherical inclusion of radius R increases like R^{-3} with decreasing radius, while the curvature increases like R^{-1}. The build-up of salt arrests the collapse through the cryoscopic relation.
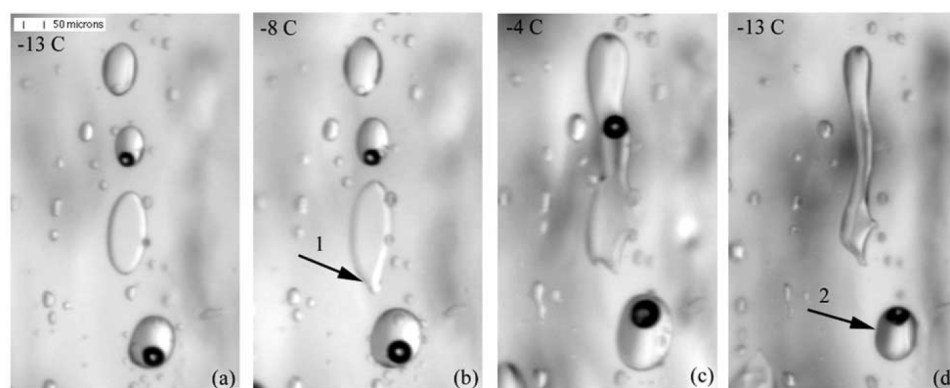
FIG. 6. *Evolution of brine inclusions in the absence of thermal gradient as the temperature was increased from* (a) −13 °C *to* (b) −8 °C *to* (c) −4 °C, *then decreased to* (d) −13 °C. *Dark circles with a bright center are air bubbles. The figure is from* [19]; *reprinted with permission from John Wiley and Sons.*

The axially symmetric quasi-steady system is computed on a cell-centered grid with $s \in [0, 1]$, a scaled arc length variable as in [22]. Finite difference approximations are used for the derivatives and the integral in (4.9) is approximated with the trapezoidal rule. The right half of the shape is computed, and ghost points [28] are used to apply the boundary and symmetry conditions. Backward Euler time stepping is implemented, and Newton iterations are performed at every time step to solve the resulting nonlinear system. A grid refinement study gave the expected convergence: first-order accuracy in time-step and second-order accuracy with respect to spatial resolution.

Figure 6 presents images from an experimental investigation of reversibility of inclusion shapes under heating cooling cycles in the absence of thermal gradients. In frame (a) the unmodified first-year sea ice has a number of vertically aligned inclusions and is held at a spatially uniform −13 °C. The sample is then uniformly heated with the outcome presented in frames (b) and (c) and then cooled back to −13 °C in frame (d). The four largest inclusions, initially ranging between 0.5 and 1 mm in diameter, increase in size, with one merging with a small inclusion at −8 °C; see arrow 1. At −4 °C three of the large inclusions merge into an extended brine tube of length 2 mm. Under reduction of temperature back to −13 °C, the tube contracts but is otherwise stable. A fundamental question is if the tube would be stable under the cooling in the presence of a thermal gradient. Indeed it is plausible that the three isolated inclusions from which the tube formed arose through the pinch-off of a tube during a cooling event in the presence of a thermal gradient. Arrow 2 indicates an isolated pocket with reversible changes under the heating and cooling cycles.

We compare the zero-gradient experimental investigates with simulations of the quasi-steady axisymmetric Stefan-type system. While this system does not support mergings, it can follow inclusion evolution up to a pinch-off singularity. As presented in Figure 7(left), we simulate a spherical brine inclusion that is initially at −2 °C with a thermal gradient of 2 °C/m. At $\tau = 1$ the system is subject to a rapid decrease in temperature to −4 °C and an increase in thermal gradient of 14 °C/m. In Figure 1, this corresponds to an inclusion located at about 1 m depth transitioning from the June 2013 to the March 2013 temperature profiles. The inclusion contracts under the reduction in temperature but remains largely spherical despite the symmetry
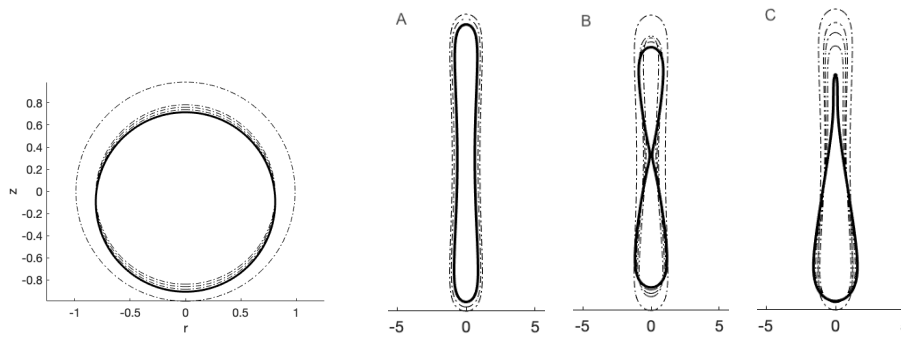
FIG. 7. *Simulation of brine inclusions showing initial and intermediate times (dotted) and final time (solid). Both horizontal and vertical axes are in millimeters, but the axes on the right are scaled compared to those on the left. Temperature and gradient are shifted at slow time $\tau = 1$ in all simulations. (Left) A spherical inclusion with temperature shifted from $-2\,^{\circ}C$ to $-4\,^{\circ}C$ and thermal gradient shifted from $2\,^{\circ}C/m$ to $14\,^{\circ}C/m$. Images are at slow time $\tau = 0, 2, 3, 4, 5$. (A) Simulation is in the absence of thermal gradient with temperature shifted from $-2\,^{\circ}C$ to $-6\,^{\circ}C$. Images at $\tau = 1, 3, 4, 5$. (B) Simulation has shift from $0\,^{\circ}C/m$ to $14\,^{\circ}C/m$ thermal gradient and temperature decreased from $-2\,^{\circ}C$ to $-10\,^{\circ}C$. Images at $\tau = 0, 1, 1.5, 2, 2.58$ (pinch-off). (C) Simulation has shift from $0\,^{\circ}C/m$ to $14\,^{\circ}C/m$ thermal gradient and temperature is decreased from $-2\,^{\circ}C$ to $-4\,^{\circ}C$. Images at $\tau = 1, 3, 4, 4.87$ (pinch-off).*

breaking induced by the temperature gradient. However the gradient induces a slow rigid-body descent corresponding to a multidimensional traveling wave solution with a velocity that is linear in the thermal gradient for values relevant to sea ice. In Figure 7(right—A, B, C) each image presents the results of three simulations, each depicting the evolution of an axisymmetric tube. In each simulation an initial inclusion was allowed to equilibrate at a given temperature under zero thermal gradient for $\tau \in (0, 1)$ before being exposed to a decrease in temperature and an increase in temperature gradient. The first simulation (A) shows the impact of a shift in temperature from $-2\,^{\circ}$C to $-6\,^{\circ}$C in the absence of a thermal gradient. This mimics the laboratory conditions of Figure 6(d). The brine tube contracts but does not pinch-off. Following the cooling the evolution slows, and the last two brine tube profiles are indistinguishable. The second simulation (B) shows the impact of a simultaneous application of a thermal gradient of $14\,^{\circ}$C/m and a shift in temperature from $-2\,^{\circ}$C to $-10\,^{\circ}$C. This corresponds roughly to a June to March transition (see Figure 1) at a depth of 0.3 m. The brine tube pinches off quickly in the middle. This suggests that a continuation beyond pinch-off would lead to the formation of a string of two or more larger brine inclusions. Significantly there is no observable downward motion in the presence of the thermal gradient, suggesting that the spatial variation of interfacial curvature at least temporarily suppresses the transition to a traveling structure. The third simulation (C) shows the impact of a simultaneous application of a thermal gradient of $14\,^{\circ}$C/m and a shift in temperature from $-2\,^{\circ}$C to $-4\,^{\circ}$C, corresponding to June to March transition at a depth of 0.8 m, near the bottom of the ice sheet. Here the evolution is slower, and the top of the brine tube contracts into a uniformly thin neck. Significantly the pinch-off initiates at the top of the tube, which suggests that a continuation beyond pinch-off would lead to a sequence of pinch-off events that produce a string of many small brine inclusions and a single large inclusion.

5. Discussion. We present a thermodynamically consistent model for the slow evolution of brine inclusions within sea ice that generates salt exclusion via the entropy of salt relative to liquid water. Adapting the classical sharp-interface scaling, a

multiscale analysis reduces the flow to a Stefan-type problem that couples the temperature and salinity to the evolution of the inclusion boundary. Numerical simulations of the quasi-steady version of the Stefan-type problem highlight the role of thermal gradients in the pinch-off of brine pores into spherical inclusions. Large gradients and warm temperatures, such as found near the bottom of the ice, may lead to pore pinch-off into a range of small and large inclusions. Large gradients and swings to colder temperatures, such as found at the top of the sea ice, may lead to pinch-off into equal sized inclusions. These observations are commensurate with Figure 3 which displays samples of brine inclusions in first-year sea ice. In both images the brine inclusions arise in vertically aligned columns that are evocative of the pinch-off of longer brine pores examined here. It is also natural to ask if thermal gradients will induce migration of brine inclusions. Interestingly, the analysis and numerics suggest that spherical inclusions are more susceptible to migration, as their constant curvature does not readily adjust to the inhomogeneity of the thermal gradient, leading to rigid-body evolution rather than the deformation that is seen in pore-type inclusions.

The model presents several opportunities for novel analysis. The combination of an L^2 gradient for the nonconserved phase, a weighted H^{-1} gradient for the conserved salt leads, and chemotactic terms arising from the relative entropy present several challenges to the analysis. Most chemotactic results have addressed spatially localized patterns, such as spikes [27]. Brine inclusions are very much a chemotactic phenomena, transporting uniformly distributed ocean salt at 3.5% weight fraction into brine inclusions at 10–20% weight fraction. However the inclusions are spatially extended patterns, with a length scale that is 10^6 times longer than the ice-liquid interface. A rigorous analysis of the stability and evolution of these spatially extended inclusions seems to require a different class of tools. A good starting point is to address the stability of traveling spherical inclusions in the presence of a thermal gradient.

The issues raised present opportunities for model calibration. Almost all laboratory work on sea ice is conducted at constant temperature, without thermal gradient. The thermal gradients in sea ice in winter are very significant. A simple point of validation would be to measure the drift speed of circular inclusions as a function of the strength of the thermal gradient or to recapitulate the work of [19], such as that presented in Figure 6, under the influence of thermal gradients.

The model contains many simplifications, some of which make it harder to incorporate experimental data into the initial model development. An obvious improvement is to consider a more physical balance between entropy and free energy for the ice-liquid transition. As discussed in the work of Penrose and Fife [24], the entropy of the phase change should be convex, with the nonconvexity that drives the spinodal decomposition appearing through the temperature dependence of the latent heat. An even more ambitious extension is to incorporate the microstructure of the ice phase and the elastic energy driven by the expansion of water upon freezing. This would require the full GENERIC framework [20]. Both of these projects are future work.

REFERENCES

[1] T. Bartels-Rausch, V. Bergeron, J. H. Cartwright, R. Escribano, J. L. Finney, H. Grothe, P. J. Gutiérrez, J. Haapala, W. F. Kuhs, J. B. Pettersson, S. D. Price, C. I. Sainz-Díaz, D. J. Stokes, G. Strazzulla, E. S. Thomson, H. Trinks,

AND N. URAS-AYTEMIZ, *Ice structures, patterns, and processes: A view across the ice-fields*, Rev. Modern Phys., 84 (2012), p. 885.

[2] G. CAGINALP, *The dynamics of a conserved phase field system: Stefan-like, Hele-Shaw, and Cahn-Hilliard models as asymptotic limits*, IMA J. Appl. Math., 44 (1990), pp. 77–94.

[3] D. M. COLE, *The microstructure of ice and its influence on mechanical properties*, Eng. Fract. Mech., 68 (2001), pp. 1797–1822.

[4] ENGINEERING TOOLBOX, *Density of aqueous solutions of inorganic sodium salts*, 2017, https://www.engineeringtoolbox.com/density-aqueous-solution-inorganic-sodium-salt-concentration-d_1957.html, [Accessed: 02.08.2021].

[5] L. EVANS, *Partial Differential Equations: Second Edition*, Graduate Studies in Mathematics, American Mathematical Society, Providence, RI, 1998.

[6] M. FABRIZIO, C. GIORGI, AND A. MORRO, *Solidification and separation in saline water*, Discrete Contin. Dyn. Syst. Ser. S, 9 (2016), pp. 139–155.

[7] D. FELTHAM, N. UNTERSTEINER, J. WETTLAUFER, AND M. WORSTER, *Sea ice is a mushy layer*, Geophys. Res. Lett., 33 (2006).

[8] K. FRANKLIN, P. MUIR, T. SCOTT, AND P. YATES, *Introduction to Biological Physics for the Health and Life Sciences*, Wiley, Hoboken, NJ, 2019.

[9] K. GOLDEN, *Brine percolation and the transport properties of sea ice*, Ann. Glaciol., 33 (2001), pp. 28–36.

[10] M. GRMELA AND H. C. ÖTTINGER, *Dynamics and thermodynamics of complex fluids. I. Development of a general formalism*, Phys. Rev. E, 56 (1997), pp. 6620–6632.

[11] M. GRMELA AND H. C. ÖTTINGER, *Dynamics and thermodynamics of complex fluids. II. Illustrations of a general formalism*, Phys. Rev. E, 56 (1997), pp. 6633–6655.

[12] R. HANDEL, R. L. DAVIDCHACK, J. ANWAR, AND A. BRUKHNO, *Direct calculation of solid-liquid interfacial free energy for molecular systems: Tip4p ice-water interface*, Phys. Rev. Lett., 100 (2008), 036104.

[13] O. HELLMUTH, J. SCHMELZER, AND R. FREITEL, *Ice-crystal nucleation in water: Thermodynamic driving force and surface tension. Part I: Theoretical foundation*, Entropy, 22 (2019), pp. 1–50.

[14] K. JUNGE, H. EICKEN, AND J. W. DEMING, *Bacterial activity at -2 to $-20°C$ in Arctic wintertime sea ice*, Appl. Environ. Microbiol., 70 (2004), pp. 550–557.

[15] D. KAHN AND J. YARBOURGH, *Chemistry: A Fundamental Overview of Essential Principles*, Cognella, San Diego, CA, 2018.

[16] V. KUMAR, A. SRIVASTAVA, AND S. KARAGADDE, *Generalized regimes for the formation of stratified regions during freezing of multi-component mixtures*, Phys. Fluids, 31 (2019), 123602.

[17] J. M. LEE, *Riemannian Manifolds: An Introduction to Curvature*, Graduate Texts in Mathematics, Springer, New York, 1997.

[18] R. M. LIEB-LAPPEN, E. GOLDEN, AND R. OBBARD, *Metrics for interpreting the microstructure of sea ice using x-ray micro-computed tomography*, Cold Reg. Sci. Technol., 138 (2017), pp. 24–35.

[19] B. LIGHT, G. MAYKUT, AND T. GRENFELL, *Effects of temperature on the microstructure of first-year Arctic sea ice*, J. Geophys. Res. Oceans, 108 (2003), 3051.

[20] A. MIELKE, *Formulation of thermoelastic dissipative material behavior using GENERIC*, Contin. Mech. Thermodyn., 23 (2011), pp. 233–256.

[21] K. MORAWETZ, S. THOMS, AND B. KUTSCHAN, *Formation of brine channels in sea ice*, Eur. Phys. J. E, 40 (2017), p. 25.

[22] I. MOYLES AND B. WETTON, *A numerical framework for singular limits of a class of reaction diffusion problems*, J. Comput. Phys., 300 (2015), pp. 308–326, https://doi.org/10.1016/j.jcp.2015.07.053.

[23] M. O'SADNICK, M. INGHAM, H. EICKEN, AND E. PETTIT, *In situ field measurements of the temporal evolution of low-frequency sea-ice dielectric properties in relation to temperature, salinity, and microstructure*, Cryosphere, 10 (2016), pp. 2923–2940.

[24] O. PENROSE AND P. C. FIFE, *Thermodynamically consistent models of phase-field type for the kinetic of phase transitions*, Phys. D Nonlinear Phenom., 43 (1990), pp. 44–62.

[25] D. K. PEROVICH, *The Optical Properties of Sea Ice*, Monograph 96-1, US Army Corps of Engineers, Cold Regions Research & Engineering Laboratory, Hanover, New Hampshire, 1996.

[26] D. PRINGLE, J. MINER, H. EICKEN, AND K. GOLDEN, *Pore space percolation in sea ice single crystals*, J. Geophys. Res. Oceans, 114 (2009), C12017.

[27] B. SLEEMAN, M. WARD, AND J. WEI, *The existence, stability, and dynamics of spike patterns in a chemotaxis model*, SIAM J. Appl. Math., 65 (2005), pp. 790–817.

[28] J. W. Thomas, *Numerical Partial Differential Equations: Finite Difference Methods*, Texts in Applied Mathematics 22, Springer-Verlag, New York, 1995.

[29] T. G. Thompson and K. H. Nelson, *Concentration of brines and deposition of salts from sea water under frigid conditions*, Am. J. Sci., 254 (1956), pp. 227–238.

[30] W. F. Weeks and S. F. Ackley, *The Growth, Structure, and Properties of Sea Ice*, in The Geophysics of Sea Ice, Springer, New York, 1986, pp. 9–164.